Review Paper | Best Paper
J. Korean Inst. Electr. Electron. Mater. Eng.
Vol. 34, No. 3, pp. 167-177 May 2021
DOI: https://doi.org/10.4313/JKEM.2021.34.3.167
ISSN 1226-7945(Print), 2288-3258(Online)

Partial Electrode Configuration as a Tool for the Precise Determination of Losses and Physical Parameters of Piezoceramics

Yoonsang Park[1], Minkyu Choi[1], Hossein Daneshpajooh[1], Timo Scholehwar[2], Eberhard Hennig[2], and Kenji Uchino[1]

[1] International Center for Actuators and Transducers (ICAT), The Pennsylvania State University, University Park, PA, 16802, United States
[2] R & D Department, PI Ceramic GmbH, Lindenstrasse, Lederhose 07589, Germany

(Received March 30, 2021; Revised April 12, 2021; Accepted April 12, 2021)

Abstract: IEEE Standard on Piezoelectricity has been utilized for decades though it has shown significant issues that prevent researchers from obtaining accurate materials coefficients. To resolve these issues, our research group recently proposed partial electrode (PE) method. PE method utilizes samples that consist of the center part covered with electrode, and the side part either covered or not covered with electrode for obtaining both intensive and extensive elastic parameters. In this review, we introduce our PE method, along with physical phenomenology and background, such as issues of IEEE standard, to bolster readers understanding of needs for developing new measurement method that can compensate the standard method. It is shown that development of the PE method not only provides technological benefits, but also gives scientific importance for the piezoelectric research community from its extremely high data accuracy.

Keywords: Piezoelectric composite, Loss determination method, Piezoelectric loss, Mechanical quality factor, Heat generation, High-power piezoelectric devices

1. INTRODUCTION

Piezoelectric devices are being utilized in a number of industries, including ultrasonic transducers [1-4], portable electronic devices like mobile phones [5,6] and digital cameras [7], and the automobile industry [8,9]. Especially, piezoelectric energy harvesting devices [10-12] are to be set on "elimination of batteries", which are classified as hazardous wastes, but recycled by less than 0.5% of 10s of Billion batteries sold per year in the world [13]. The major problem of piezoelectric devices is that further miniaturization of piezoelectric devices is limited by "heat generation", owing to the "losses" in piezoelectric materials [14-16]. Meanwhile, loss values are implemented in finite element analysis (FEA) computer simulation [17-19], which is an effective tool to investigate output performance of piezoelectric devices. Therefore, obtaining accurate loss data is important for both technological and scientific assets by contributing to more accurate FEA simulation results and elucidation of heat generation mechanism in high-power piezoelectric devices.

In this review, the partial electrode (PE) method, which is parameter determination method for piezoelectric materials that our group recently developed [20,21], will be discussed.

✉ **Yoonsang Park; yup15@psu.edu**

First, necessary physical phenomenology and background will be explained to boost readers' understanding for the necessity to develop a new measurement method for piezoelectric measurement. After that, our recent achievements for developing the new measurement method will be reviewed.

2. THEORY/BACKGROUND

2.1 Intensive vs. extensive quantities and their effect on piezoelectricity

According to International Union of Pure and Applied Chemistry (IUPAC) [22], intensive quantities are those that depend on the size of the system, whereas extensive quantities are those that are independent of the size of the system. For piezoelectric materials, intensive quantities, such as stress (X) and electric field (E), are externally controllable, while extensive quantities, such as strain (x) and dielectric displacement (D), are the ones that are intrinsically determined by the material itself. The Piezoelectric constitutive relationships, in terms of both intensive and extensive quantities, can be written as [23]:

$$\begin{pmatrix} x \\ D \end{pmatrix} = \begin{pmatrix} s^E & d \\ d & \varepsilon_0 \varepsilon^X \end{pmatrix} \begin{pmatrix} X \\ E \end{pmatrix} \tag{1}$$

$$\begin{pmatrix} X \\ E \end{pmatrix} = \begin{pmatrix} c^D & -h \\ -h & (\frac{1}{\varepsilon_0})\kappa^x \end{pmatrix} \begin{pmatrix} x \\ D \end{pmatrix} \tag{2}$$

where ε^X is stress (X) constant relative dielectric permittivity (unitless), s^E is electric field (E) constant elastic compliance (in m^2/N), d is piezoelectric constant (in C/N), κ^x is strain (x) constant relative inverse permittivity (unitless), c^D is dielectric displacement (D) constant elastic stiffness (in N/m^2), and h is inverse piezoelectric coefficient (in N/C). The former three coefficients are considered as being intensive, whereas the latter three are considered as being extensive. From the constitutive equations [equation (1) and (2)], the definition of electromechanical coupling factor (k) is induced:

$$k^2 = \frac{\text{multiplication of off} - \text{diagonal terms}}{\text{multiplication of diagonal terms}} = \frac{d^2}{s^E(\varepsilon_0 \varepsilon^X)} \; or \; \frac{h^2}{s^D(\kappa^x/\varepsilon_0)} \tag{3}$$

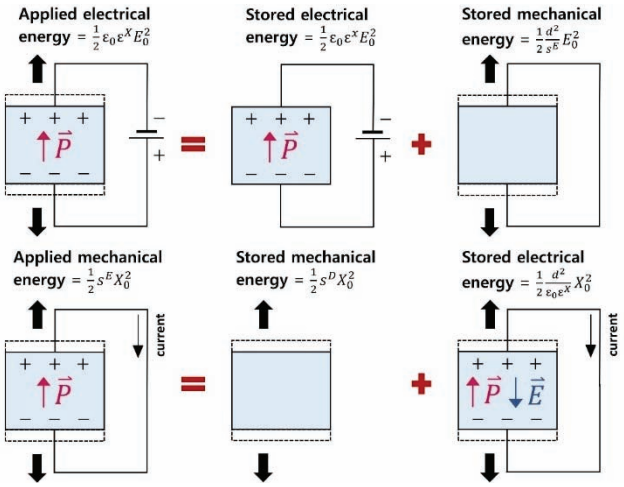

Fig. 1. Schematic diagram for relationships between different electrical/mechanical boundary conditions in piezoelectric materials in static condition. Redrawn from [24].

The relationships between different boundary conditions determined from intensive and extensive quantities in "static situation" are schematically shown in Fig. 1. For the converse piezoelectric effect (electric field generates strain) shown in the upper part of Fig. 1, the applied electrical energy ($\frac{1}{2}\varepsilon_0\varepsilon^X E_0^2$) is superposed by the sum of stored electrical energy in 3D-clamped condition ($\frac{1}{2}\varepsilon_0\varepsilon^x E_0^2$) and the mechanical energy ($\frac{1}{2}\frac{d^2}{s^E}E_0^2$) due to piezoelectricity. For direct piezoelectric effect (stress creates charge or "polarization") shown in the lower part of Fig. 1, the input mechanical energy ($\frac{1}{2}s^E X_0^2$) is superposed by the sum of stored mechanical energy in electrically open circuit condition ($\frac{1}{2}s^D X_0^2$) and electrical energy ($\frac{1}{2}\frac{d^2}{\varepsilon_0\varepsilon^X}X_0^2$) due to piezoelectricity.

The relationship described in Fig. 1 can be mathematically represented as the following equations:

$$\varepsilon_0\varepsilon^X = \varepsilon_0\varepsilon^x + \frac{d^2}{s^E} \tag{4}$$

$$s^E = s^D + \frac{d^2}{\varepsilon_0\varepsilon^X} \tag{5}$$

With the definition of k and equation (4) and (5), the relationship between intensive and extensive coefficients can be derived:

$$\frac{\varepsilon^x}{\varepsilon^X} = \frac{s^D}{s^E} = (1 - k^2) \tag{6}$$

The physical meaning of k in piezoelectricity is:

$$k^2 = \frac{stored\ mechanical\ energy}{input\ electrical\ energy}\ or \\ \frac{stored\ electrical\ energy}{input\ mechanical\ energy} \tag{7}$$

Note, however, that the above argument is accurate in the 1D model, and that the relationship should be modified in the 3D configuration as we will introduce in the later section (such as partially clamped elastic loss, $\tan\phi_{33}'''$).

2.2 Electrical boundary conditions for elasticity in piezoelectric materials

In Section 2.1, the relationships have been discussed between different boundary conditions determined from intensive and extensive quantities in "static situation" and "no size constraint" conditions. Since many piezoelectric devices in particular size constraints (plate, disk, rod etc.) are operated, those surface boundary conditions must also be discussed. Here, the discussion is limited to elastic parameters, since the dynamical (such as resonance) situation is mainly related to elastic parameters, rather than dielectric parameters that are usually determined from static or pseudo-static situation.

The *E*- or *D*- constant condition in dynamical situation can be discriminated by the presence of "depolarization field effect" [23], which is one of the most important phenomena in piezoelectricity. Depolarization field refers to the electric field that created by surface charges and negatively proportional to induced polarization P ($E_{dep} = -P/\varepsilon_0\varepsilon_r$). Let us first consider Gauss's law from Maxwell's equation [25]:

$$\nabla \cdot D = \rho_f \quad or \quad \nabla \cdot E = \frac{1}{\varepsilon_0\varepsilon_r}\left(\rho_f - \nabla \cdot P\right) \\ = \frac{1}{\varepsilon_0\varepsilon_r}\left(\rho_f - \rho_b\right) \tag{8}$$

where ρ_f and ρ_b are free and bound charges, respectively. Gauss's law in equation (8) describes electrostatic relationship for static E and D (without time-domain) created by charge distribution. However, the velocity of sound in piezoelectric medium is far lower than the speed of light; therefore, the dynamic situation of piezoelectric media can be explained by electrostatics. Accordingly, the effect of magnetic field is neglected, considering Faraday's law of induction. This assumption is called quasi-electrostatic approximation [23]. Note also that the polarization above is merely due to the induced one associated with the stress distribution, and that the spontaneous polarization is out of this discussion, so that even quartz can be discussed in the same fashion.

Let us then consider that the piezoelectric specimen shown in Fig. 2(a) for typical k_{31} mode (transverse extension) with electrode on the top and the bottom with polarization perpendicular to electrode. If the specimen is mechanically excited by AC stress along the plate length direction (our PE configuration corresponds to this mechanical excitation), mechanical vibration will be generated, which causes dynamical polarization modulation along the perpendicular direction of the specimen via d_{31}. For the simplicity, with the sinusoidal stress like the fundamental resonance mode, the tensile stress generated at the center (positive) and the induced polarization will head toward the bottom, considering the negative value of d_{31} coefficient (d_{31} is usually negative in perovskite piezoelectrics, but it is positive in ferroelectric polymer PVDF, polyvinylidene difluoride [26,27]). Since top and bottom parts are covered by electrode, the free charges in the electrode metal move and neutralize induced surface bound charges caused by the polarization. Therefore, since surface charges are neutralized, there is no depolarization field, and the elasticity is considered to be in *E*- constant condition. In this specific case, the elastic compliance is s_{11}^E (wave propagation is perpendicular to direction of polarization, which is denoted by 3).

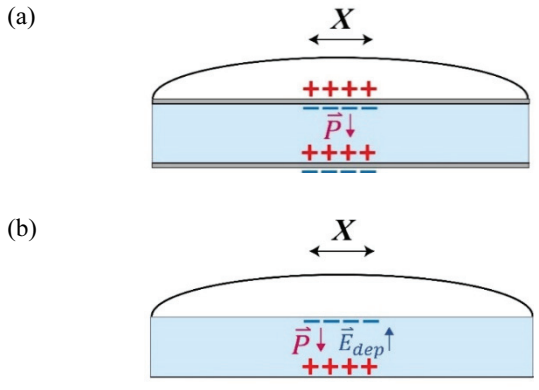

Fig. 2. (a) *E*- constant and (b) *D*- constant in k_{31} mode type vibration.

Let us next consider k_{31} mode specimen with no electrode, as shown in Fig. 2(b), where no charge neutralization is expected at the surface of the specimen. Once mechanically-excited, the bound charges generated on the specimen surface will generate so-called depolarization field to compensate the induced polarization, because the + and – charge distance (plate thickness) is quite small in the k_{31} type geometry. Therefore, the depolarization field ($E_{dep} = -P/\varepsilon_0\varepsilon_r$) is maintained to provide *D*- constant condition on elasticity. Therefore, the elastic compliance becomes s_{11}^D.

On the other hand, the standard k_{33} mode, as illustrated in Fig. 3, exhibits different surface boundary conditions. For standard k_{33} mode case shown in Fig. 3(a), even though the right and left edges are covered by electrodes (long distance between the electrodes), there is no electrode along the wave propagation direction. Thus, no charges are available to compensate the dynamical polarization modulation along the wave propagation direction (i.e., plate length), and the sound velocity along the polarization direction becomes a *D*- constant sound velocity with elastic compliance of s_{33}^D. However, it is noteworthy to mention that situation is quite different when the driving frequency is DC or pseudo-DC. When the operating frequency is low (quasi-static), the depolarization field attracts "stray" charges in the specimen or on the specimen surface from the surrounding atmosphere, and charge screening happens (usually a couple of minutes in usual cm size samples). Then, the compliance would approach to s_{33}^E.

E- constant condition for k_{33} mode in dynamical situation can be achieved when electrode is formed on the length part, as shown in Fig. 3(b). This geometry is not practically achievable since the electrode on the side will completely short the entire surface by being connected with the edge electrodes to provide equipotential to both edges. If side is covered by electrode, it will neutralize the polarization modulation in wave propagation direction, as long as the plate thickness is narrow enough. Therefore, there is no depolarization field and *E*- constant elastic compliance (s_{33}^E) can be directly obtained. The above electroded/non-electroded and k_{31}/k_{33} configurations are adopted in our PE specimen designs to measure *E*- and *D*- constant elastic compliances.

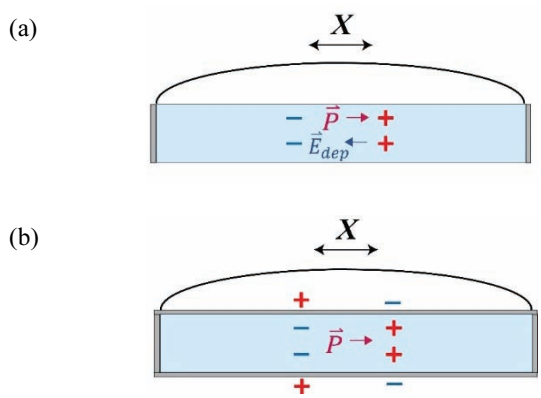

Fig. 3. (a) *D*- constant and (b) *E*- constant in k_{33} mode type vibration.

2.3 Losses in piezoelectric materials

So far, the discussion has been limited to piezoelectric phenomenology without loss. The materials' coefficients discussed in section 2.1 are often represented as complex variables (with superscripted stars) and can be represented as the following [28]:

$$\varepsilon^{X*} = \varepsilon^X(1 - j\tan\delta') \tag{9}$$

$$s^{E*} = s^E(1 - j\tan\phi') \tag{10}$$

$$d^* = d(1 - j\tan\theta') \tag{11}$$

$$\kappa^{x*} = \kappa^x(1 + j\tan\delta) \tag{12}$$

$$c^{D*} = c^D(1 + j\tan\phi) \tag{13}$$

$$h^* = h(1 + j\tan\theta) \tag{14}$$

The imaginary parts of the complex coefficients in terms of tangent angles in above equations are called losses (Throughout this paper, the real parts of these coefficients are named as physical parameters, though there are several terms to describe them). The above complex expressions including losses were based on materials' viscous damping that reflects response phase lag to the input drive force. The complex expressions in equations (9)~(11) contain intensive physical parameters and losses (primed), whereas those in equations (12)~(14) contain extensive physical parameters and losses (non-primed). The negative signs for intensive losses and positive signs for extensive losses are due to convention, considering the direction of loss hysteresis loop.

The relationship between intensive and extensive losses (though it is not applicable in some specific vibration modes like k_{33} mode) can also be related with k, as intensive and extensive parameters are related as shown in section 2.1. It is 3×3 matrix called K- matrix that relates two types of losses, which is defined as [29,30]:

$$\begin{bmatrix}\tan\delta' \\ \tan\phi' \\ \tan\theta'\end{bmatrix} = [K]\begin{bmatrix}\tan\delta \\ \tan\phi \\ \tan\theta\end{bmatrix} \tag{15}$$

$$[K] = \begin{bmatrix}1 & k^2 & -2k^2 \\ k^2 & 1 & -2k^2 \\ 1 & 1 & -1-k^2\end{bmatrix} \tag{16}$$

The matrix is mathematically proven to be "invertible", meaning that $[K]^2 = \mathrm{I}$ and $[K] = [K]^{-1}$. In usual cases, extensive losses are indirectly determined by using K- matrix from determined intensive losses. The above argument is correct only in the 1D model as in the case of E- and D- constant discussion. For k_{33} mode, the situation is quite different, in that K- matrix cannot be utilized directly to obtain the intensive loss factors, as we will detail later.

2.4 Issues of IEEE standard

The standard method to determine losses was previously established by Institute for Electrical and Electronics Engineer (IEEE) in 1980s [31]. However, there are several deficits in this method that prevent users from obtaining accurate parameters. For example, IEEE Standard excludes existence of "piezoelectric loss", which is the key factor for heat generation mechanism. The absence of piezoelectric loss is well manifested in IEEE standard's equivalent circuit (EC), as shown in Fig. 4. The damped capacitance (C_0) is parallelly connected with motional inductance (L_1), capacitance (C_1) and resistance (R_1). The mechanical quality factor (Q_m) is calculated by the following equation:

$$Q_m = \frac{\sqrt{L_1/C_1}}{R_1} \tag{17}$$

The expression of Q_m given by the equation above assumes at mechanical quality factors at resonance (Q_A) and antiresonance (Q_B) frequencies are the same. However, this assumption shows discrepancies with experimental results, in that Q_B is always larger than Q_A in lead zirconate titanate (PZT) [16,32]. Previously, our research group showed that the difference between Q_A and Q_B is due to piezoelectric loss [33] and higher Q_B due to piezoelectric loss causes less heat generation for antiresonance drive than resonance drive of k_{31} mode piezoelectric specimen under high-power conditions [16]. For k_{31} mode specimen, Q_A and Q_B are given by the following equations [33]:

$$Q_A = \frac{1}{\tan\phi'_{11}} \tag{18}$$

$$\frac{1}{Q_B} = \frac{1}{Q_A} - \frac{1}{1+\left(\frac{1}{k_{31}}-k_{31}\right)^2\Omega_B^2}(2\tan\theta'_{31} - \tan\delta'_{33} - \tan\phi'_{11}) \tag{19}$$

Where Ω_B is normalized antiresonance angular frequency, which is given by:

$$\Omega_B = \frac{\omega_B l}{2}\sqrt{\rho s_{11}^E} \tag{20}$$

Therefore, piezoelectric loss plays an important role for heat generation in high-power piezoelectric applications. To measure the piezoelectric loss factor, we need to measure simultaneously both Q_A and Q_B precisely.

The other significant issue of IEEE standard is related to k_{33} mode particular specimen (longitudinal extension). Due to its intrinsic structure, the impedance of the bar is in general high, so that it may cause huge experimental error and electrical noise, especially near antiresonance frequency (maximum resistance point). Figure 5 shows electrical response

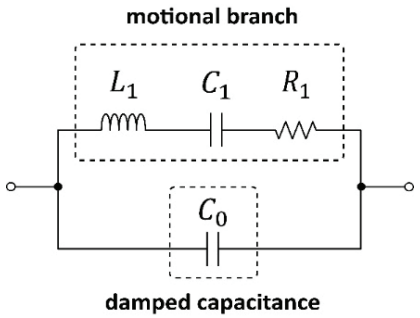

Fig. 4. Equivalent circuit (EC) of a piezoelectric vibrator given by IEEE standard.

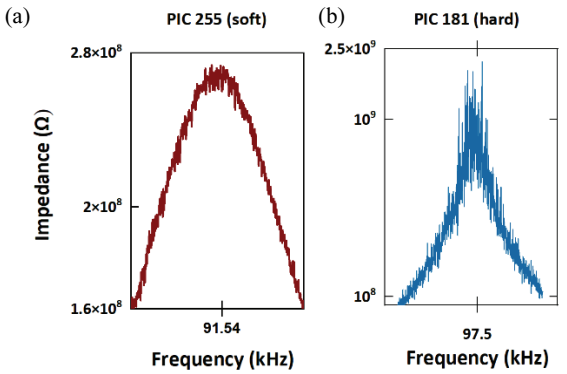

Fig. 5. Impedance curves near antiresonance frequency of standard k_{33} specimens composed of (a) PIC 255 [21] and (b) PIC 181 near half power bandwidth (bandwidth with 3 dB points).

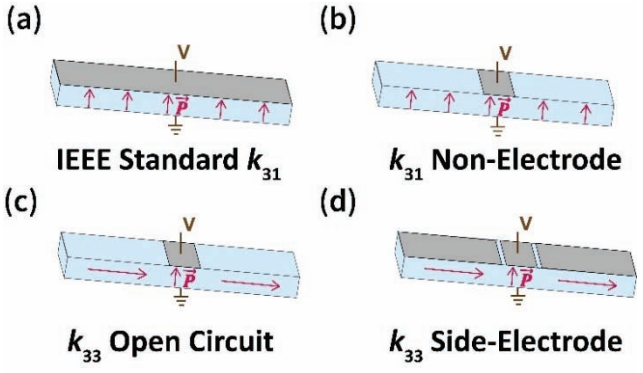

Fig. 6. Sample geometries of (a) standard k_{31} specimen, (b) k_{31} mode PE non-electrode (NE), (c) k_{33} mode PE open circuit (OC), and (d) k_{33} mode PE side electrode (SE). Redrawn from [37].

(impedance peak around the antiresonance frequency) of k_{33} mode specimen composed of PIC 181 (hard) and PIC 255 (soft) under the constant AC voltage drive of IEEE standard k_{33} mode samples composed of PIC 181 (hard) and PIC 255 (soft), with the dimension of 20×2.5×0.5 mm^3. As shown in Fig. 5(a), even with soft PZT that has relatively small Q_B (~ 100), electrical noise is manifest. The noise issue near Q_B becomes more serious in the case of hard PZT, as shown in Fig. 5(b).

For k_{33} mode specimens, there are more issues; the issues include fringing electric field, and specimen setup issue [21]. Furthermore, only one type of elastic compliance and loss can be determined from each type of vibration mode. For instance, while k_{31} mode specimen provides only *E*- constant elastic compliance and loss, k_{33} mode specimen provides only *D*- constant elastic compliance and loss.

2.5 Partial electrode (PE) configuration as the solution

In order to resolve such disadvantages of IEEE standard, several measurement methods have been employed, such as samples with polarization angle rotation [34] and pulse echo method [35,36]. Partial electrode (PE) method is also one of the methods that was devised due to the same motivation. PE method basically utilizes the PE configuration which is a plate structure that is composed of electrically excited and measured center part and the mechanically excited side parts, as shown in Fig. 6(b), (c) and (d). Since the purpose of PE configuration is to characterize properties of the side part, center part is maintained to about 10% of the length of plate, whereas side parts take up about 90% of the entire length. This characterization methodology is based on mechanical excitation, which is different from electrical excitation method suggested by IEEE standard. The measurement is done through the center part with capacitance about 200 times larger than IEEE standard, considering the same sample's aspect ratio of the dimension [21]. Therefore, the measurements do not suffer from small capacitance or high impedance issue. It also enables characterization of both intensive and extensive losses simply by covering the side part with electrode or not, respectively. Moreover, with mechanical excitation, it is possible to characterize unpoled piezoelectric materials, which cannot be electrically excited due to zero piezoelectricity.

3. METHODOLOGY

3.1 k_{31} and k_{33} mode characterization

PE method utilizes curve fitting technique to obtain physical parameters and losses. Experimental admittance or impedance curves are fitted to analytical solutions that were derived for PE configuration structure. The admittance analytical solution is composed of two parts, which are damped and motional branch. The damped branch is described by the following equation:

$$Y_{d,PE} = \frac{j\omega\varepsilon_{33}^{X*}\left(1 - {k_{31}}^{*2}\right)alw}{t} \quad (21)$$

Where ω is angular frequency ($\omega = 2\pi f$), l, w and t are length, width, and thickness of PE plate, respectively, and a is center portion, ranging from 0 to 1 (0 to 100%). Note that materials' coefficients are represented as complex variables to include loss parts. The motional branch is described as follow [37]:

$$Y_{m,PE} = \frac{jw}{t}\frac{2d_{31}^{*2}}{s_{11}^{E*2}}\left[\frac{1}{\left[\rho v_{11}^{E*}cot\left(\frac{a\omega l}{2v_{11}^{E*}}\right) - \rho v_{side}^{*}tan\left(\frac{(1-a)\omega l}{2v_{side}^{*}}\right)\right]}\right] \quad (22)$$

Where v_{side}^{*} is complex sound velocity of side part ($v_{side}^{*} = 1/\sqrt{\rho s_{side}^{*}}$). The complex elastic compliances of side part (s_{side}^{*}) can be s_{11}^{D*} (for k_{31} NE), s_{33}^{D*} (for k_{33} OC) or s_{33}^{E*} (for k_{33} SE) depending on side parts' poling and electrode configuration. For the complex elastic compliances, the corresponding losses are $\tan\phi_{11}$, $tan\,\phi_{33}'''$ and $tan\,\phi_{33}'$, respectively. Note that $tan\,\phi_{33}'''$ is extensive-like loss (not 100% extensive, but rather close), due to 3D constraint condition (partially clamped elastic condition). $\tan\phi_{33}$, which is extensive loss and can be obtained from fully 3D-clamped condition, is obtained by measuring standard thickness mode (k_t) samples.

For motional branch, to separate center and side parts' contribution, impedance equation is more useful:

$$Z_{m,PE} = \frac{-jt}{w}\frac{s_{11}^{E*2}}{2d_{31}^{*2}}\left[\rho v_{11}^{E*}cot\left(\frac{a\omega l}{2v_{11}^{E*}}\right) - \rho v_{side}^{*}tan\left(\frac{(1-a)\omega l}{2v_{side}^{*}}\right)\right] \quad (23)$$

In equation (23), the first term (cotangent function) inside the square bracket is motional contribution from the center part, whereas the second term (tangent function) is motional contribution from the side part. The analytical solutions were validated with FEA computer simulation with exactly same input parameter values. Since the analysis is done with the analytical solutions with 1D assumption, it is highly recommended that l, w and t should satisfy the following relationship: $l >> w >> t$. In our previous works [18,21], we prepared PE samples that have dimensions of 20×2.5×0.5 mm^3.

To determine physical parameters and losses related to k_{31} and k_{33} modes, the following steps describe parameter determination process using standard k_{31} mode samples and PE samples. It is noteworthy to mention that standard k_{31} mode specimen is included in the process, since it does not have any particular issue and is reliable to do electrical measurement on.

1. The dimensions (l, w, t), mass (ρ) of all the samples (k_{31} specimens + PE specimens), and the center portion (a) for PE specimens are measured for each sample. The mass and dimension measurements are essential step for any piezoelectric specimen measurement.
2. Admittance/impedance data of standard k_{31} mode samples at fundamental resonance are measured with an impedance analyzer, and parameters (s_{11}^{E*}, ε_{33}^{X}, d_{33}^{*}, k_{31}^{*}) are obtained by the method described in Zhuang [33]. The physical parameters and losses determined from standard k_{31} mode samples for both hard and soft PZT are shown in Table 1.
3. Admittance/impedance curves of PE specimens (k_{31} NE, k_{33} OC, and k_{33} SE) are measured with an impedance analyzer, and complex elastic compliances are obtained with nonlinear regression curve fitting using the admittance equations [equation (18) and (19)]. Because the center part of the PE specimen is k_{31} mode, k_{31} mode-related parameters determined in step 2 can be plugged into analytical solution to minimize the fitting variables. Therefore, for each PE specimen, 2 parameters (elastic compliance and corresponding elastic loss of side part) can be determined.
4. Electromechanical coupling factor of k_{33} mode (k_{33}) and its piezoelectric constant (d_{33}) are determined from the following two equations:

$$k_{33} = \sqrt{1 - \frac{s_{33}^{D}}{s_{33}^{E}}} \quad (24)$$

$$d_{33} = k_{33}\sqrt{\varepsilon_0\varepsilon_{33}^{X}s_{33}^{E}} \quad (25)$$

5. Finally, intensive piezoelectric loss ($\tan\theta_{33}'$) and coupling loss ($\tan\chi_{33}$) can be determined using the following equation:

Table 1. Physical parameters and losses determined from standard k_{31} mode samples made of hard (PIC 181) and soft (PIC 255) PZT ceramics. Data taken from [37].

	PIC 181	PIC 255
ε_{33}^{X} (…)	1,263±3	1,934±3
s_{11}^{E} (10^{-12} m^2/N)	11.94±0.03	16.77±0.04
d_{31} (pC/N)	-121.4±0.4	-194.7±0.5
$\tan\delta'_{33}$ (%)	0.362±0.003	1.54±0.01
$\tan\phi'_{11}$ (%)	0.054±0.001	1.21±0.02
$\tan\theta'_{31}$ (%)	0.239±0.004	2.26±0.04

$$\tan\theta'_{33} = \frac{1}{2k_{33}^2}[tan\,\phi'_{33} - (1-k_{33}^2)\,tan\,\phi'''_{33} + k_{33}^2\,tan\,\delta'_{33}] \quad (26)$$

$$\tan\chi_{33} = 2\tan\theta'_{33} - tan\,\delta'_{33} - tan\,\phi'_{33} \quad (27)$$

In addition, proper dielectric calibration is necessary to ensure good fittings. Because measured center part is parallelly sandwiched between two side parts that have similar magnitude of dielectric permittivity, the damped admittance is overestimated by fringing electric field. The calibration can be done by measuring dielectric permittivity via center part of PE specimens and evaluate degree of fringing effect.

3.2 Elastic characterization of unpoled piezoceramics

To ensure high performance, several piezoelectric devices, such as multilayer actuators [38], piezoelectric voltage transformers [39-42] and ultrasonic motors [43] require complex electrode or poling configurations. In the process of multiple poling steps and during the device operation with high power, those devices obtain partially poled or completely unpoled regions. Furthermore, several piezoelectric devices, such as energy-trapped piezoelectric oscillators [44], piezoelectric micromachined ultrasonic transducers (pMUT) [45] and actuators utilizing shear modes [46] have majority of volumes that consist of unpoled segments. Since partially poled or unpoled segments show different physical properties from the poled piezoelectric materials, it is imperative to elucidate related physics, as well as to determine accurate physical parameters and losses to properly devise piezoelectric devices with desired output performance using FEA computer simulation.

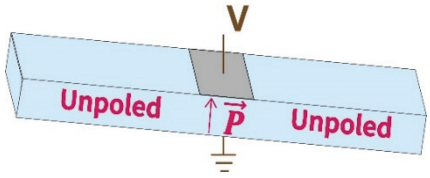

Fig. 7. PE configuration with unpoled side part for elastic measurement of unpoled piezoelectric materials. Redrawn from [47].

Because unpoled piezoelectric materials are less useful for technological applications, their materials' properties have not been paid attention. This indifference may have caused lack of reported materials' coefficient of unpoled piezoelectric materials. Usually, experimentally obtaining dielectric permittivity and dielectric loss is relatively straightforward, since they can directly be measured with LCR meters or impedance analyzers near off-resonance frequency (usually 1 kHz). However, obtaining elastic compliance and elastic loss causes certain level of experimental hardship, because unpoled piezoelectric materials cannot be electrically excited to create mechanical resonance.

Using PE configuration with unpoled side part, as shown in Fig. 7, our group could determine complex elastic compliance of unpoled piezoelectric ceramics [47]. The parameter determination process is quite similar to PE method for k_{31} and k_{33} modes described in section 3.1. The admittance equation of PE configuration with unpoled side part is of the same form as equation (19). By performing curve fitting on experimental data of PE specimens with unpoled side parts using the same analytical solution, elastic compliance and elastic loss of unpoled piezoelectric materials can be obtained.

4. RESULTS AND DISCUSSIONS

4.1 k_{31} and k_{33} mode parameters

Table 2 shows k_{33} mode-related physical parameter and loss values determined from standard k_{33} mode samples and

Table 2. Physical parameters and losses determined from standard k_{33} mode samples and PE samples made of PIC 255. Data taken from [21].

	PIC 255 (IEEE standard)	PIC 255 (PE)
s_{33}^D ($\times 10^{-12}$ m^2/N)	8.30±0.06	9.21±0.02
s_{33}^E ($\times 10^{-12}$ m^2/N)	17.8±0.4	17.70±0.04
d_{33} (pC/N)	390±10	382±1
k_{33} (%)	73±1	69.3±0.1
$tan\,\phi_{33}'''$ (%)	0.5±0.1	0.56±0.01
$tan\,\phi_{33}'$ (%)	1.2±0.6	1.20±0.02
$\tan\theta_{33}'$ (%)	1.8±1.2	1.80±0.01
$\tan\chi_{33}$ (%)	0.6±2.8	0.70±0.02

Table 3. Physical parameters and losses determined from PE samples made of hard (PIC 181) and soft (PIC 255) PZT ceramics. Data taken from [37].

	PIC 255 (PE)	PIC 181 (PE)
s_{11}^D ($\times 10^{-12}$ m^2/N)	14.30±0.05	10.53±0.05
s_{33}^D ($\times 10^{-12}$ m^2/N)	9.68±0.03	8.53±0.04
s_{33}^E ($\times 10^{-12}$ m^2/N)	17.5±0.1	13.03±0.06
d_{33} (pC/N)	365±5	224±2
k_{33} (%)	66.8±0.1	58.8±0.4
$tan\,\phi_{11}$ (%)	0.87±0.01	0.039±0.001
$tan\,\phi_{33}'''$ (%)	0.51±0.01	0.030±0.001
$tan\,\phi_{33}'$ (%)	1.19±0.01	0.053±0.002
$\tan\theta_{33}'$ (%)	1.79±0.02	0.229±0.003
$\tan\chi_{33}$ (%)	0.85±0.04	0.043±0.007

PE samples. Note that values determined from IEEE standard have huge error range, in particular, in loss factors, due to that electrical noise fluctuation was considered. Since the noise fluctuation has more effect on quality factors rather than resonance/antiresonance frequencies, $tan\,\phi_{33}'''$ has relatively huge error range compared to real parameter s_{33}^D and error propagation amplifies the errors for the other loss values due to error propagation.

Table 3 shows physical parameter and loss values determined from standard k_{31} samples and PE samples. Note slightly different values from the PE samples made of PIC 255, because the sample sets are from different bulk ceramic blocks. With determined parameters from standard k_{31} samples and PE samples, the following relationships have been found:

1. Regardless of the type of piezoelectric materials (either soft or hard PZT), the coupling loss ($\tan\chi_{31}$ and $\tan\chi_{33}$), which is imaginary part of k^2, is always positive. This means that Q_B>Q_A; the relationship denotes that twice the piezoelectric loss is always larger than the sum of dielectric and elastic loss ($2\tan\theta' > \tan\delta' + \tan\phi'$). In some lead-free piezoelectric materials, such as NKN*, it was found that Q_A>$Q8_B$ (i.e. $2\tan\theta' < \tan\delta' + \tan\phi'$)*.
2. The soft PZT (PIC 255) samples has higher permittivity and piezoelectric constants, compared to hard PZT (PIC 181) samples. This is because the chemical doping for soft PZT is designed to facilitate domain wall motions to obtain high permittivity and piezoelectric constants. However facilitate domain wall motions negatively affect soft PZT by increasing loss values. The all anisotropic dielectric, elastic, piezoelectric loss values of PIC 255 are higher than those of PIC 181.
3. For all types of piezoelectric materials studies here, the inequality relationship $s_{33}^D < s_{11}^D < s_{11}^E < s_{33}^E$ was obtained. This means that extensive elastic compliances are more stiffening than intensive ones. Similar inequality relationship can also be found from intensive and extensive elastic losses, though the magnitude of intensive losses in 11 and 33 directions are very similar.

4.2 Elastic "intermediacy" of unpoled piezoelectric materials

Table 4 shows elastic compliance and elastic loss of unpoled soft (PIC 255) and (PIC 181) hard PZT ceramics. With the intensive and extensive elastic compliance and loss values of k_{31} and k_{33} mode, the following relationship is induced:

1. $s_{33}^D < s_{11}^D < s_{eff} < s_{11}^E < s_{33}^E$
2. $\tan\phi_{33}''' < \tan\phi_{11} < \tan\phi_{eff} < \tan\phi_{11}' \approx \tan\phi_{33}'$

From the inequality relationships above, it is concluded that complex elastic compliance of unpoled piezoelectric ceramic is not simply an average of s_{33}^{D*} and s_{11}^{D*} (average of elastic compliance for cases with no electrode) but lies in between intensive and extensive elasticity. This is different from the simple intuition that the physical parameters of unpoled piezoelectric materials should be average of poled materials.

Table 4. Effective elastic compliance and elastic loss of unpoled hard (PIC 181) and soft (PIC 255) PZT ceramics. Data taken from [47].

PIC 181		PIC 255	
s_{eff} (10-12 m^2/N)	11.07±0.07	s_{eff} (10-12 m^2/N)	14.58±0.02
$tan\,\phi_{eff}$ (%)	0.042±0.002	$tan\,\phi_{eff}$ (%)	0.97±0.01

This elastic intermediacy of unpoled piezoelectric ceramic was interpreted in our recent report [47] with simplified assumption that each grain is considered as being a mesoscale single crystal with multidomain state. Each domain in a grain retains spontaneous polarization and generates depolarization field. In this case, there are two possibilities for charge configuration: the surface bound charges between two adjacent grains have the same sign ('+ to +' or '– to –') or opposite sign ('+ to –'). If the charges with the same signs are paired, domains experience *D*- constant condition because depolarization field still exists, whereas the charges with the opposite signs leads to *E*- constant, since depolarization field is cancelled out due to charge neutralization.

5. CONCLUSION

In this review, the PE method for loss and physical parameter determination of piezoelectric materials has been discussed. The physical phenomenology related to intensive and extensive quantities and the issues of IEEE standard on piezoelectricity were explained to provide readers background for necessity of devising new measurement method. By resolving issues of IEEE and providing more reliable ways of loss determination, (1) the PE method can contribute to accurate determination of loss values for technological, in particular, 200 times higher capacitance for the k_{33} measurement. (2) *E*- and *D*- constant parameters can be measured with the same geometry specimens just by coating the electrode on the surface. (3) a new scientific discovery was made, in that elasticity of unpoled piezoelectric materials shows "intermediacy" between intensive-ness and extensive-ness. The new scientific finding on the precise loss date by our PE measurement not only promotes fundamental understandings of piezoelectric materials' domain dynamics, but also contributes to design and optimization of various state-of-the-art piezoelectric devices.

ORCID

Yoonsang Park https://orcid.org/0000-0002-2492-1328

ACKNOWLEDGEMENT

This work was supported by Office of Naval Research with Grant Number N00014-17-1-2088 and N00014-20-1-2039.

REFERENCES

[1] A. Abdullah, M. Shahini, and A. Pak, *J. Electroceram.*, **22**, 369 (2009). [DOI: https://doi.org/10.1007/s10832-007-9408-8]

[2] X. Dong, T. Yuan, M. Hu, H. Shekhani, Y. Maida, T. Tou, and K. Uchino, *Rev. Sci. Instrum.*, **87**, 105003 (2016). [DOI: https://doi.org/10.1063/1.4963920]

[3] S. Hirose, M. Aoyagi, and Y. Tomikawa, *Jpn. J. Appl. Phys.*, **32**, 2418 (1993). [DOI: https://doi.org/10.1143/jjap.32.2418]

[4] A. Iula, F. Vazquez, M. Pappalardo, and J. A. Gallego, *Ultrasonics*, **40**, 513 (2002). [DOI: https://doi.org/10.1016/s0041-624x(02)00174-9]

[5] O. D. Kwon, J. S. Yoo, Y. J. Yun, J. S. Lee, S. H. Kang, and K. J. Lim, *Proc. 2005 International Symposium on Electrical Insulating Materials, 2005. (ISEIM 2005)* (IEEE, Kitakyushu, Japan, 2005) p. 676. [DOI: https://doi.org/10.1109/iseim.2005.193460]

[6] H. P. Ko, H. Jeong, and B. Koc, *J. Electroceram.*, **23**, 530 (2009). [DOI: https://doi.org/10.1007/s10832-008-9529-8]

[7] D. S. Paik, K. H. Yoo, C. Y. Kang, B. H. Cho, S. Nam, and S. J. Yoon, *J. Electroceram.*, **22**, 346 (2009). [DOI: https://doi.org/10.1007/s10832-008-9513-3]

[8] Y. Zhang, R. Zheng, K. Shimono, T. Kaizuka, and K. Nakano, *Sensors*, **16**, 1727 (2016). [DOI: https://doi.org/10.3390/s1610 1727]

[9] S.T.A. Hamdani and A. Fernando, *Sensors*, **15**, 7742 (2015). [DOI: https://doi.org/10.3390/s150407742]

[10] C. Sugino and A. Erturk, *J. Phys. D: Appl. Phys.*, **51**, 215103 (2018). [DOI: https://doi.org/10.1088/1361-6463/aab97e]

[11] S. Priya, H. C. Song, Y. Zhou, R. Varghese, A. Chopra, S. G. Kim, I. Kanno, L. Wu, D. S. Ha, J. Ryu, and R. G. Polcawich, *Energy Harvesting Syst.*, **4**, 3 (2019). [DOI: https://doi.org/10.1515/ehs-2016-0028]

[12] H. S. Kim, J. H. Kim, and J. Kim, *Int. J. Precis. Eng. Manuf.*, **12**, 1129 (2011). [DOI: https://doi.org/10.1007/s12541-011-0151-3]

[13] Battery Market, *Growth, Trends, COVID-19 Impact, and Forecasts (2021 - 2026)* https://www.mordorintelligence.com/industry-reports/global-battery-market-industry (2019, Accessed

March 29th 2021).

[14] J. Zheng, S. Takahashi, S. Yoshikawa, K. Uchino, and J.W.C. de Vries, *J. Am. Ceram. Soc.*, **79**, 3193 (1996). [DOI: https://doi.org/10.1111/j.1151-2916.1996.tb08095.x]

[15] Y. H. Su, Y. P. Liu, D. Vasic, W. J. Wu, F. Costa, and C. K. Lee, *IEEE Trans. Ultrason. Ferroelectr. Freq. Control*, **59**, 2129 (2012). [DOI: https://doi.org/10.1109/tuffc.2012.2439]

[16] S. O. Ural, S. Tuncdemir, Y. Zhuang, and K. Uchino, *Jpn. J. Appl. Phys.*, **48**, 056509 (2009). [DOI: https://doi.org/10.1143/jjap.48.056509]

[17] S. Dong, S. P. Lim, K. H. Lee, J. Zhang, L. C. Lim, and K. Uchino, *IEEE Trans. Ultrason. Ferroelectr. Freq. Control*, **50**, 361 (2003). [DOI: https://doi.org/10.1109/tuffc.2003.1197958]

[18] Y. Park, M. Majzoubi, Y. Zhang, T. Scholehwar, E. Hennig, and K. Uchino, *J. Appl. Phys.*, **127**, 204102 (2020). [DOI: https://doi.org/10.1063/1.5143728]

[19] E. Heinonen, J. Juuti, and S. Leppävuori, *J. Eur. Ceram. Soc.*, **25**, 2467 (2005). [DOI: https://doi.org/10.1016/j.jeurceramsoc.2005.03.083]

[20] M. Majzoubi, H. N. Shekhani, A. Bansal, E. Hennig, T. Scholehwar, and K. Uchino, *J. Appl. Phys.*, **120**, 225113 (2016). [DOI: https://doi.org/10.1063/1.4971340]

[21] Y. Park, Y. Zhang, M. Majzoubi, T. Scholehwar, E. Hennig, and K. Uchino, *Sens. Actuators, A*, **312**, 112124 (2020). [DOI: https://doi.org/10.1016/j.sna.2020.112124]

[22] M. Nic, J. Jirat, and B. Kosata, Compendium of Chemical Terminology, International Union of Pure and Applied Chemistry (IUPAC) (2014) p. 542, p. 740.

[23] T. Ikeda, *Fundamentals of Piezoelectricity* (Oxford University Press, New York, 1990) pp. 54-82.

[24] K. Uchino, *Advanced Piezoelectric Materials, Elsevier* (Woodhead Publishing, Cambridge, UK, 2017) p. 647. [DOI: https://doi. org/10.1016/b978-0-08-102135-4.00017-5]

[25] D. J. Griffiths, *Introduction to Electrodynamics, 4th ed.* (Cambridge University Press, Cambridge, UK, 2017) pp. 167-202. [DOI: https://doi.org/10.1017/9781108333511]

[26] V. Ostaševičius, I. Milašauskaitė, R. Daukševičius, V. Baltrušaitis, V. Grigaliūnas, and I. Prosyčevas, *Mechanics*, **86**, 78 (2010).

[27] G. M. Sessler and A. Berraissoul, *IEEE Trans. Electr. Insul.*, **24**, 249 (1989). [DOI: https://doi.org/10.1109/14.90283]

[28] Y. Zhuang, S. O. Ural, S. Tuncdemir, A. Amin, and K. Uchino, *Jpn. J. Appl. Phys.*, **49**, 021503 (2010). [DOI: https://doi.org/10.1143/jjap.49.021503]

[29] H. Daneshpajooh, H. N. Shekhani, M. Choi, and K. Uchino, *J. Am. Ceram. Soc.*, **101**, 1940 (2018). [DOI: https://doi.org/10.1111/jace.15338]

[30] K. Uchino, Y. Zhuang, and S. O. Ural, *J. Adv. Dielectr.*, **1**, 17 (2011). [DOI: https://doi.org/10.1142/s2010135x11000033]

[31] A. Meitzler, H. Tiersten, A. Warner, D. Berlincourt, G. Couqin, and F. Welsh III, *IEEE Standard on Piezoelectricity* (IEEE Ultrasound, Ferroelectrics and Frequency Control Society, New York, USA, 1988) pp. 29-63.

[32] A. V. Mezheritsky, *IEEE Trans. Ultrason. Ferroelectr. Freq. Control*, **49**, 484 (2002). [DOI: https://doi.org/10.1109/58.996567]

[33] Y. Zhuang, S. O. Ural, and K. Uchino, *Ferroelectrics*, **470**, 260 (2014). [DOI: https://doi.org/10.1080/00150193.2014.923727]

[34] M. Choi, Y. Park, H. Daneshpajooh, T. Scholehwar, E. Hennig, and K. Uchino, *Ceram. Int.*, (In press, 2021). [DOI: https://doi.org/10.1016/j.ceramint.2021.02.210]

[35] H. Cao, V. H. Schmidt, R. Zhang, W. Cao, and H. Luo, *J. Appl. Phys.*, **96**, 549 (2004). [DOI: https://doi.org/10.1063/1.1712020]

[36] R. Zhang, B. Jiang, and W. Cao, *Appl. Phys. Lett.*, **82**, 787 (2003). [DOI: https://doi.org/10.1063/1.1541937]

[37] Y. Park, H. Daneshpajooh, T. Scholehwar, E. Hennig, and K. Uchino, Physical Parameter and Loss Determination Using Partial Electrode: k_{31} and k_{33} Mode Cases, ArXiv e-Print (2020).

[38] Y. Shindo, F. Narita, and M. Hirama, *Smart Mater. Struct.*, **18**, 085020 (2009). [DOI: https://doi.org/10.1088/0964-1726/18/8/085020]

[39] P. Laoratanakul, A. V. Carazo, P. Bouchilloux, and K. Uchino, *Jpn. J. Appl. Phys.*, **41**, 1446 (2002). [DOI: https://doi.org/10.1143/jjap.41.1446]

[40] C. A. Rosen, Ph.D. Dissertation, Analysis and Design of Ceramic Transformers and Filter Elements, Syracuse University, New York (1956).

[41] E. M. Syed, F. P. Dawson, and E. S. Rogers, *Proc. 2001 IEEE 32nd Annual Power Electronics Specialists Conference (IEEE Cat. No. 01CH37230)* (IEEE, Vancouver, Canada, 2001) p. 1761. [DOI: https://doi.org/10.1109/pesc.2001.954377]

[42] H. Xue, J. Yang, and Y. Hu, *IEEE Trans. Ultrason. Ferroelectr. Freq. Control*, **55**, 1632 (2008). [DOI: https://doi.org/10.1109/tuffc.2008.837]

[43] G. L. Smith, R. Q. Rudy, R. G. Polcawich, and D. L. DeVoe, *Sens. Actuators, A*, **188**, 305 (2012). [DOI: https://doi.org/10.1016/j.sna.2011.12.029]

[44] A. Ando, T. Kittaka, Y. Sakabe, and S. Fujishima, Energy-Trapping-Type Piezoelectric Resonance Device, Google Patents, 1990.

[45] Y. Qiu, J. V. Gigliotti, M. Wallace, F. Griggio, C.E.M. Demore, S. Cochran, S. Trolier-McKinstry, *Sensors*, **15**, 8020 (2015). [DOI: https://doi.org/10.3390/s150408020]

[46] S. W. Bartky, A. D. Paton, S. Temple, and J. A. Michaelis, Pulsed Droplet Deposition Apparatus Using Unpoled Crystalline Shear Mode Actuator, Google Patents, 1991.

[47] Y. Park, H. Daneshpajooh, T. Scholehwar, E. Hennig, and K. Uchino, *Appl. Mater. Today*, **23**, 101020 (2021). [DOI: https://doi.org/10.1016/j.apmt.2021.101020]